

Article

Influence of Electron Beam Treatment of Co–Cr Alloy on the Growing Mechanism, Surface Topography, and Mechanical Properties of Deposited TiN/TiO₂ Coatings

Stefan Valkov ^{1,*}, Stoyan Parshorov ², Andreana Andreeva ³, Ruslan Bezdushnyi ³, Maria Nikolova ⁴, Dimitar Dechev ¹, Nikolay Ivanov ¹ and Peter Petrov ¹

¹ Institute of Electronics, Bulgarian Academy of Sciences, 72 Tzarigradsko Chaussee Blvd, 1784 Sofia, Bulgaria

² Institute of Metal Science, Equipment and Technologies with Hydro- and Aerodynamics Centre, Bulgarian Academy of Sciences, 67, Shipchenski Prohod Blvd, 1574 Sofia, Bulgaria

³ Faculty of Physics, Sofia University, 5 James Bourchier Blvd, 1164 Sofia, Bulgaria

⁴ Department of Material Science and Technology, University of Ruse, 8 Studentska Str., 7017 Ruse, Bulgaria

* Correspondence: stsvalkov@gmail.com

Received: 9 July 2019; Accepted: 10 August 2019; Published: 13 August 2019



Abstract: This study examines the effect of electron beam treatment (EBT) of Co–Cr substrate on the film growth mechanism, mechanical properties, and surface topography of TiN/TiO₂ coatings deposited by reactive magnetron sputtering. The obtained results and processes that occurred during the deposition are discussed in the context of crystallographic principles, and special attention is paid to the crystallographic orientation and growth mechanism studied by X-ray diffraction (XRD). The mechanical properties were investigated by means of nanoindentation and wear tests. The surface topography was evaluated using atomic force microscopy (AFM). The results obtained in the present study showed that polycrystalline TiN and anatase TiO₂ phases were present in all cases. Electron beam treatment of Co–Cr substrate tended to form a reorientation of the microvolumes from (111) to (200) of TiN, leading to a change in the growth mechanism from three-dimensional (Volmer–Weber) to layer-by-layer (Frank–van der Merwe). It was found that the electron beam treatment process did not significantly affect the thickness of the coatings and the deposition rate. The treatment process led to an increase in surface roughness. The higher surface roughness after the EBT process should be appropriate to support cell growth and adhesion on the surface of the deposited bilayer coating. It was demonstrated that EBT of the substrate caused a decrease in hardness of the deposited coatings from 10 to 5 GPa. The observed decrease in hardness was attributed to the change in the preferred crystallographic orientation and film growth mechanism. The hardness of the bilayer coating after the application of EBT of the Co–Cr substrate was much closer to that of human bones, which means that severe stress shielding effect could not be expected. The evaluated coefficient of friction (COF) exhibited significantly lower values in the case of EBT of the substrate compared to the untreated Co–Cr material.

Keywords: electron beam modification; magnetron sputtering; multilayer TiN/TiO₂ coatings; X-ray diffraction; atomic force microscopy; nanoindentation

1. Introduction

Co–Cr alloys have a number of applications due to their good corrosion resistance, attractive mechanical properties, and biocompatibility. These materials have received a lot of attention in the field of implant manufacturing [1–3]. However, they have some drawbacks related to low wear

resistance, which depends mostly on the surface properties and can be overcome by appropriate surface modification technologies [4].

During the last decades, considerable attention has been paid to surface manufacturing of materials by high-energy fluxes (HEFs) (i.e., electron and laser beams). In these technologies, the electrons or photon fluxes interact with the surface of the sample, heat the treated area, and form a thermal distribution. The rate of heating and cooling can be characterized by quite high values (about 10^5 – 10^6 K/s), which lead to some structural changes in the functional properties [5–10]. The authors of [11] demonstrated an innovative approach for controlling the surface topography and tribological behavior of biomedical alloys, such as Ti6Al4V, by means of electron beam surface treatment. Other researchers [12,13] have successfully demonstrated the possibilities for enhancing the wear and corrosion properties of steel by the formation of carbon fiber-reinforced Ni-based composite coatings via laser cladding. Laser beam technologies have a large number of applications in the field of modern medicine and are extensively discussed in [10].

Other methods for coating deposition are plasma spray technologies, physical vapor deposition (PVD), etc. It should be noted that magnetron sputtering (MS), as a part of PVD processes, is a promising technology due to the possibility of controlling the structure and properties of the obtained coatings and is appropriate for deposition of nitride and oxide-based films [14–18].

Titanium nitride (TiN) films, deposited on different substrates, have many applications in modern human life because of their exceptional mechanical properties, resistance to corrosion, wear resistance, etc. Titanium dioxide (TiO₂) is another material that can be applied in the form of a coating and is characterized by enhanced biocompatibility. Such TiO₂ coatings have a number of applications as biomedical materials. There have been various studies describing the deposition and investigation of TiN and TiO₂ coatings. The authors of [19] studied the mechanical, tribological, and biological properties of TiN coatings deposited on Ti6Al4V substrate. Their results showed that the deposited coating was seven times harder than the substrate and that the wear rate of TiN was four orders of magnitude lower than that of the Ti6Al4V alloy. The same authors concluded that the deposited TiN coatings were biocompatible and nontoxic [19]. Pham et al. [20] studied TiN coatings deposited on Co–Cr substrate and discussed the potential application of TiN deposited on Co–Cr as a vascular stent due to the 1.3 times higher culturing of endothelial cells compared to the uncoated substrate. The authors of [21–23] based their work on modification of the structure and properties of differently deposited coatings. Chen et al. [22] developed a plasma gun-based remelting method for modification of the structure and properties of sprayed NiCrBSi coatings, and their results showed that the remelting process led to a reduction in porosity, formation of metallurgical bonding between the coating and substrate, and an increase in hardness and wear resistance. Similarly, the authors of [21] studied the influence of short-time heat treatment of plasma-sprayed NiCrBSi coatings on their structure and properties, and the results showed an increase of over 15% in hardness and about 60% in wear resistance. In another study [23], a duplex modification of steel substrate by deposition of TiAlN coating and subsequent electron beam treatment (EBT) was carried out. The deposition of the coating led to an enhancement in absorption properties of the base material and a significant increase in hardness compared to the same electron beam treatment of uncoated steel.

Based on the performed literature review, it is obvious that the technologies discussed above are capable of improving the functional properties of different materials. Although the authors of [20] studied the structure and properties of deposited TiN coatings on Co–Cr substrate, a combination of treatment using high-energy fluxes and coating deposition to overcome the discussed drawbacks of Co–Cr alloy has not yet been studied. As already mentioned, by using HEFs for surface treatment of materials, their structure and properties can be modified. On the other hand, the film growth mechanism of the deposited coatings strongly depends on the structure and properties of the substrate material and greatly influences the functional properties of the deposited coatings.

The aim of the present study was to investigate the growth mechanism of bilayer TiN/TiO₂ coatings onto Co–Cr alloys deposited by direct current (DC) magnetron sputtering. The influence

of electron beam treatment of the substrate on the growth mechanism, mechanical properties, and surface topography of bilayer TiN/TiO₂ was extensively studied. The results relating to hardness, surface roughness measurements, and wear performance are discussed with respect to the electron beam modification process and film growth mechanism.

2. Materials and Methods

Multilayer TiN/TiO₂ coatings were deposited on Co–Cr alloy (25.5 wt % Cr; 0.2 wt % Mn; 4.3 wt % Fe; 59.5 wt % Co; 1.0 wt % Ni; 4.7 wt % Mo; 0.6 wt % W; 4.3 wt % others). Before the deposition, a substrate with a diameter of 20 mm and thickness of 3 mm was grounded and mirror-polished by conventional metallographic techniques. Half of the samples underwent electron beam treatment before the deposition. During the EBT process, the following technological parameters were applied: accelerating voltage, 52 kV; electron beam current, 25 mA; electron beam scanning frequency, 1 kHz; speed of the specimen motion, 4 cm/s; and diameter of the electron beam, 0.5 mm. The discussed technological conditions were selected in order to reach the highest cooling rate without melting the surface of the Co–Cr substrate during treatment. The temperature during the treatment process on the surface of the electron beam-modified specimen was evaluated according to a numerical model published elsewhere [24,25]. It was found that the sample was heated to about 1350 °C by applying the discussed technological parameters. A scheme of the EBT process is presented in Figure 1.

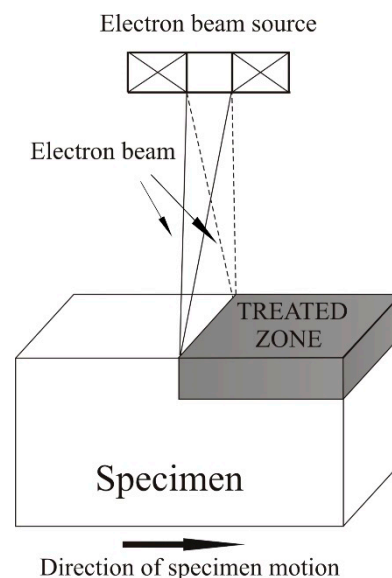


Figure 1. Sketch of the electron beam treatment experiment.

The multilayer coating deposition was deposited by reactive magnetron sputtering, where the purity of the Ti target was 99.8%. The deposition of the TiN layer was carried out in Ar–N₂ atmosphere at a working pressure of 1.2×10^{-1} Pa and 23:1 Ar:N₂ ratio, and the substrate was heated up to 350 °C. The TiO₂ film was obtained in pure O₂ atmosphere and working pressure of 7×10^{-2} Pa, and the substrate temperature was decreased from 350 down to 180 °C. Negative bias voltage to the substrate was not applied. The TiN film was deposited for 1.5 h and TiO₂ for 2 h. The discussed technological conditions of bilayer coating deposition were optimized in order to obtain stoichiometrical and monophasic TiN and TiO₂ films.

The phase composition and crystallographic orientation of the deposited coatings were studied by means of X-ray diffraction (XRD, URD 6 Seifert & Co diffractometer, GmbH, Ahrensburg, Germany). The experiments were realized within the range of 20°–70° at 2 θ scale with a step of 0.1° and counting time of 10 s per step. All measurements were conducted in a symmetrical Bragg–Brentano (B–B) mode.

The film thickness was determined from optical cross-sectional images of both polished and electron beam-treated coated samples via software on a large scale.

The depth profiles of Ti, N, and O were measured by glow discharge optical emission spectroscopy (GDOES, GDS-750 QDP, LECO Instruments, St. Joseph, MI, USA) under conventional plasma conditions.

The nanosurface topology was studied by means of atomic force microscopy (High-speed AFM, Anfatec Instruments AG, Oelsnitz, Germany). The experiments were performed in noncontact mode, where the curvature radius of the silicon nitride tip was 10 nm. A small-size scanned area of 20 $\mu\text{m} \times 20 \mu\text{m}$ along the x - and y -axes was chosen, and 512 measurements of the heights were taken at each of these directions (i.e., 512 \times 512 measured points for the area).

The hardness of the deposited films was studied by means of a nanomechanical tester (Bruker, Billerica, MA, USA). The experiment consisted of a total of 48 indentations (4 lines with 12 indentations each) with spacing of 80 μm and applied load of 50 mN.

The coefficient of friction (COF) was measured by micromechanical wear test ball-on-flat with hardened sliding ball coated with Cr. The measurements were carried out for 600 s with a load of 2 N at room temperature.

3. Results and Discussion

Figure 2 presents the experimentally obtained XRD patterns of both treated and untreated coated specimens. All diffraction maxima were indexed. There were some peaks belonging to the Co substrate as well as to the TiN and TiO₂ from the coatings. It was clear that, before the treatment process, the phase composition of the substrate consisted of a mixture of ϵ -Co and γ -Co. The presence of double-phase structure before the surface treatment can be explained by a reaction of γ -Co \rightarrow ϵ -Co, which occurred at 880 °C during the cooling process. After the EBT, it was transformed into a single-phase structure of γ -Co. It should be noted that cobalt exists in two allotropic forms: ϵ -Co, which has a hexagonal close-packed (hcp) structure and appears at low temperatures, and γ -Co, which has a face-centered cubic (fcc) structure and is stable at high temperatures. The Gamma cobalt phase is known as a high-temperature modification of the material, and the discussed fcc structured phase is also known to be unstable at room temperature. However, Granqvist et al. [26] mentioned that it can exist in the form of ultrafine particle structure. It is known that treatment techniques by high-energy fluxes are capable of finer microstructure formation. This statement is in agreement with the results obtained for the phase composition of the substrate with and without electron beam treatment. Furthermore, the authors of [27,28] mentioned that the transition from γ to ϵ phases during cooling after the manufacturing process is sluggish, and some traces of fcc structure can be found. During electron beam surface modification, the cooling rate is quite high, and the discussed transformation from hcp to fcc does not occur as the transition process is sluggish. Similar results were obtained by the authors of [29], where a Co–Cr alloy implant was subjected to laser interface lithography modification. This is completely in agreement with our results, where the treatment processing of the substrate surface formed a single-phase structure of γ -Co.

Except for reflections from the substrate polycrystalline, TiN and TiO₂ phases from the coatings were registered. TiN has an fcc lattice, and several structural types of TiO₂ exist, including β -TiO₂, anatase (a-TiO₂), rutile (r-TiO₂), etc. The obtained patterns show the presence of a-TiO₂.

The preferred crystallographic orientation of the phases from the coatings was studied quantitatively via P_{hkl} pole density, which is proportional to the probability of a particular family of crystallographic planes being parallel to the surface, and is given by Equation (1):

$$P_{hkl} = \frac{I_{hkl}^{exp} / I_{hkl}^{st}}{\frac{1}{n} \sum_n I_{hkl}^{exp} / I_{hkl}^{st}} \quad (1)$$

In Equation (1), I^{exp} and I^{st} are the experimentally obtained and standard ICDD intensities, respectively; and n is the number of the considered diffraction peaks. The results are summarized in Table 1. In the case of the deposited TiN/TiO₂ coatings on untreated Co–Cr substrate, a predominant (111) crystallographic texture at TiN layer was observed. After the substrate treatment by a high-intensity electron flux, the contribution of (111) texture dropped from about 64% to 27%, while (200) increased from about 31% up to 61%, therefore becoming predominant. Thus, a reorientation in the microvolumes from (111) to (200) of TiN was observed after the EBT process. Concerning the TiO₂ phase, no significant differences in the crystallographic orientations were observed. In both cases, (200) was predominant, and after the treatment, the values of P_{hkl} decreased from 66% to 55%.

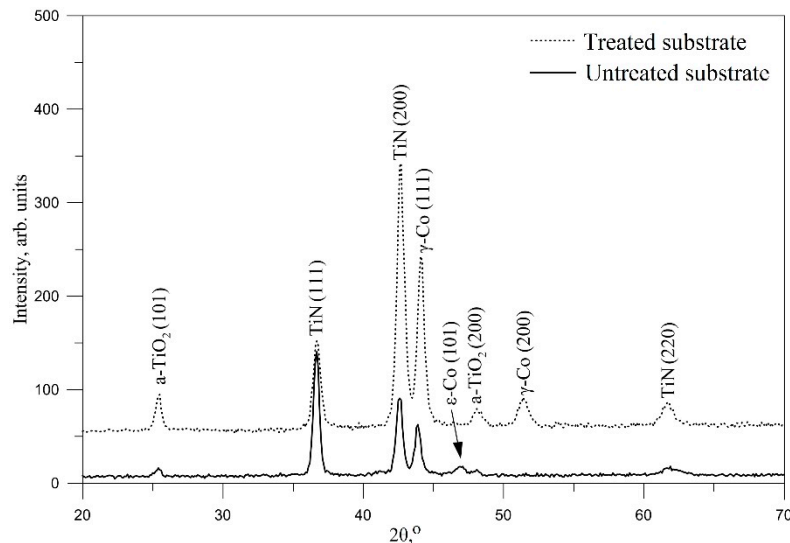


Figure 2. XRD pattern of the deposited coatings on electron beam-treated and untreated Co–Cr substrate.

Table 1. The shares of microvolumes of different texture components evaluated by P_{hkl} .

Substrate Processing	TiN			TiO ₂	
	P_{111} , %	P_{200} , %	P_{220} , %	P_{101} , %	P_{200} , %
Untreated	64.32	31.18	4.50	45.11	54.89
EBT	27.12	61.25	11.63	33.69	66.31

The appearance of preferred crystallographic orientation in magnetron-sputtered TiN films has been extensively discussed in [30]. The authors of [30] based their discussion on the nature of the selection of the preferential crystal plane where the densest is privileged. They can be separated into three groups. The first is (311) and (111), which consist of only Ti atoms; the second is (222), which has only N atoms; and the third is (220) and (200), which are composed of a mixture of Ti and N atoms. They are ordered with respect to their density as follows: (311), which has the least density; (111) and (222), which have equal densities; (220); and (200), which has the most density. Thus, the preferred orientation should be in the (200) direction. However, the plane density is not the only factor for preferred film growth. The thermal agitation energy due to substrate heating and the energy of atoms when they fall on the substrate or on the growing film are also of great interest. With regard to Ti atoms, their energy is relatively high because they come directly from the target. For N atoms, two different cases exist: (i) some of them react with the Ti target and are then sputtered and have similar energy as Ti atoms; (ii) some come from the gaseous phase, and their energy is much lower than that of Ti. It should be noted that the nitrogen atoms, which react with Ti target and are subsequently sputtered, are almost entirely responsible for the formation of TiN molecule. Those coming from the gaseous phase have much smaller energy, and the probability of incorporating into TiN lattice is very small; as a result, they are mostly located at the grain boundaries [30]. The lower substrate temperature leads to

low thermal agitation energy, and only a small amount of atomic rearrangement can occur, leading to a small amount of N atoms in the TiN lattice. Therefore, in the case of Ti-rich TiN film, the predominant orientation will be the densest one that contains only Ti atoms, i.e., (111). An increase in the substrate temperature and thermal agitation energy will result in an increase in atomic mobility and atomic rearrangement, respectively. This will lead to a greater occupation of TiN lattice with nitrogen, and the preferred crystallographic orientation will be transformed to the densest plane that contains both Ti and N atoms, i.e., (200) [30].

These statements are in agreement with the results obtained in the present study. It is known that during the deposition of coatings by magnetron sputtering, except for the external heating, the substrate is warmed up to a certain temperature due to the following reasons: (i) the kinetic energy of the atoms of deposited material; (ii) the release of energy during the condensation and crystallization of the film; and (iii) the energy of the secondary electrons emitted from the target. [31]. On the other hand, as already mentioned, the EBT of Co–Cr substrate leads to a phase transformation from $\epsilon + \gamma$ to γ . Glagoleva et al. [32] studied the thermal properties of Co–Cr alloys and showed that the thermal conductivity of the γ phase is lower than that of the ϵ -phase within the temperature range of 600–1700 K. Therefore, during the deposition process, the surface consisting of a single gamma-phase structure (treated substrate) is heated more vigorously than the substrate containing a mixture of $\epsilon + \gamma$ phases (untreated substrate). Furthermore, the injection of electrons during the treatment process can be another reason for the increase in the thermal conductivity of the substrate after the EBT process. Thus, the reorientation of microvolumes from (111) to (200) of TiN film is in correlation with the texture formation theory and the thermal properties of the Co–Cr substrate [30,32]. According to the authors of [33], for magnetron-sputtered TiN coatings, nuclei differing in their crystallographic orientation are formed via different growth mechanisms. When the nuclei are oriented parallel to the substrate surface with (111) crystallographic planes, Volmer–Weber mechanism of nucleation (three-dimensional nucleation from the beginning of the film growth) is realized [33]. At the same time, nuclei that are orientated parallel to the substrate surface with (100) or (110) crystallographic planes are formed via layer-by-layer Frank–van der Merwe mechanism [33]. Therefore, electron beam treatment of Co–Cr substrate led to different growth mechanism of the TiN layer. The EBT of the base material led to a change in the growth mechanism from the three-dimensional Volmer–Weber to the layer-by-layer Frank–van der Merwe mechanism.

Concerning both diffraction patterns shown in Figure 2, no amorphous-like halos were observed, indicating a high degree of crystallinity of the samples (i.e., the Co–Cr substrates and the deposited bilayer coatings in both cases). Also, in the case of EBT of the substrate, the peaks were stronger and narrower, indicating a lower concentration of the crystallographic imperfections. During the growth of the bilayer coating on the untreated substrate, the mobility of the atoms in the growing layer was relatively low due to the lower temperature on the surface of the substrate, unlike in the case of EBT of the substrate, where the energy and mobility of the growing particles were higher. The diffusion processes caused redistribution and even partial annihilation of the imperfections.

The overall thickness of the deposited coatings on electron beam-treated and untreated Co–Cr substrates were evaluated by cross-sectional optical analysis. The results revealed that both EBT and polished samples had an almost identical overall thickness equal to 0.94 ± 0.05 and 1.04 ± 0.04 μm , respectively. This means that the treatment process did not significantly affect the deposition rate. Nevertheless, the authors of [34] showed that TiN surface with (200) orientation exhibits much more affinity to oxidation and provides available sites for oxygen molecule adsorption. This means that the zone between the nitrogen and oxygen part of the coating (i.e., the oxynitride region) should be larger due to the diffusion of oxygen on the surface of the TiN layer. The (200) TiN allows higher deposition rate, meaning that the thickness of the oxide–nitride layer should be a bit larger in the case of a deposition on a treated substrate compared to an untreated one. These statements are in correlation with our XRD results, which showed that the diffraction maxima of the TiO_2 phase were stronger in the case of the EBT substrate compared to the untreated substrate.

The change in the average concentration of Ti, N, and O through the thickness of the coatings was measured by GDOES analysis, and the results are shown in Figure 3. The compositional depth profile of Ti/O ratio was close to the stoichiometrically correct values (33 at % Ti and 66 at % O) for TiO₂. The oxygen content decreased gradually from the surface until it reached 3 at %–4 at % in the nitride. This indicates that the residual oxygen present in the vacuum chamber during sputtering was in competition with reactive gas for Ti adsorption site occupancy. Another source of O could be that in the vacuum chamber during spectra acquisition. The average atomic concentration of N in TiN was in the range of 38%–40%, and the N/Ti ratio was about 0.7 or a little lower than the stoichiometry expected ratio. Low content of carbon (1%–2%) was also observed at the surface of the deposits. The thickness of the oxide was less than 0.1 μm, whereas the oxynitride zone was commensurate with the oxide thickness.

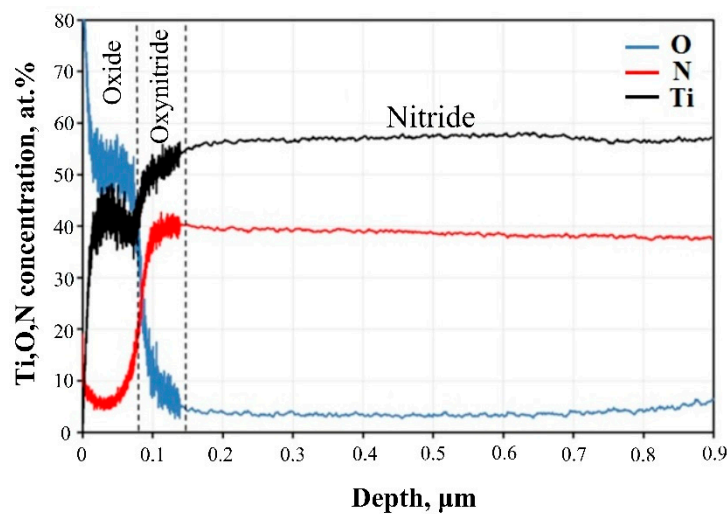


Figure 3. Depth profiles of Ti, O, and N in TiN/TiO₂ coating deposited on Co–Cr substrate without electron beam treatment.

Both samples showed almost similar depth profiles of the elements with lower than stoichiometry N/Ti ratio of the nitride. The intensities of element distribution normally show considerable scattering in concentration vs. depth quantification, especially for samples with a rough surface like that of the electron beam-treated sample. For this reason, and because of the small coating thickness, the results from EBT and coated sample are not presented here.

Figure 4 presents two- and three-dimensional AFM images of the surface topography of the bilayer coatings deposited on the electron beam-treated and untreated Co–Cr substrate. The influence of the EBT process on the topography of the surfaces of the investigated samples was quantitatively evaluated by the so-called mean roughness value S_a , which is calculated according to Equation (2):

$$S_a = \frac{1}{M \times N} \sum_{k=0}^{M-1} \sum_{l=0}^{N-1} |z(x_k, y_l) - \mu| \quad (2)$$

In Equation (2), M and N are the numbers of the measured points along the x - and y -axes, z is the height at the point with coordinates x_k and y_l ; and μ is the mean height.

The results obtained for the mean roughness parameter are summarized in Table 2. It is obvious that the electron beam treatment of Co–Cr material led to about 3 times increase in the surface roughness. The authors of [35] mentioned that the electron beam treatment of smooth surfaces is capable of forming craters and increasing the roughness. According to another research [36], an electron beam treatment of smooth surfaces results in an increase in roughness because, during the treatment process, a small amount of material is evaporated, followed by condensation, which leads to a formation of

protrusions [36]. Therefore, it can be concluded that EBT of smooth surfaces will lead to an increase in surface roughness. These statements are in agreement with the results obtained in our study, where electron beam treatment of previously polished Co–Cr substrate resulted in an increase in the surface roughness. The higher measured values of the S_a parameter of the bilayer TiN/TiO₂ in the case of electron beam-treated substrate are due to the fact that the topography of the deposited coatings follows the topography of the covered material. With regard to the roughness, the calculated S_a values are commonly accepted as low-roughness surface texturing. The nanosized topographic profiles on the implant surface may be of practical importance with respect to wettability, cell adhesion, adsorption of proteins, and biomineralization phenomenon [37]. It was shown by Zhou et al. [38] that the percentage of fully spread epithelial-like cells among attached cells and cell density on 13 nm rough magnetron-sputtered TiO₂ coating was higher after 16 h of incubation compared to 5 nm rough coated samples. Furthermore, considering the crystalline structure of the obtained oxide, this anatase crystal architecture would be more beneficial for decreased bacterial proliferation because it has been found that amorphous TiO₂ promotes bacterial attachment [39]. Colon et al. reported that, in contrast to the microstructured surface, nanostructured TiO₂ reduced *Staphylococcus epidermidis* adhesion and increased osteoblast functions, alkaline phosphatase activity, and calcium mineral deposition [40].

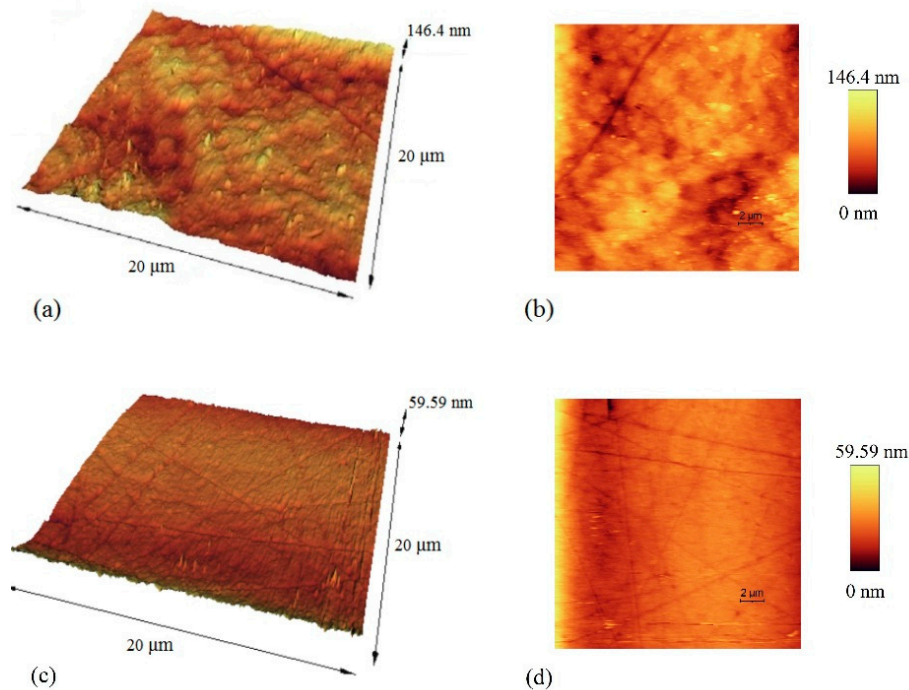


Figure 4. Atomic force microscopy (AFM) 2D and 3D images of TiN/TiO₂ coating deposited on Co–Cr substrate: (a) 3D micrograph of treated substrate; (b) 2D micrograph of treated substrate; (c) 3D micrograph of untreated substrate; (d) 2D micrograph of untreated substrate.

Table 2. The parameters characterizing the surface topography (S_a), thickness, hardness (H), and coefficient of friction (COF) of the investigated samples.

Substrate Processing	S_a (nm)	Thickness (μm)	H (GPa)	COF
Untreated	5.10 ± 0.01	1.04 ± 0.04	10.706 ± 0.580	0.653 ± 0.222
EBT	14.96 ± 0.04	0.94 ± 0.05	5.030 ± 0.895	0.241 ± 0.105

The influence of EBT on the hardness of the surface of both samples was investigated by nanoindentation, and the results are presented in Table 2. Figure 5 presents the experimentally obtained load–displacement curves from which the hardness values were evaluated [41,42]. It is obvious that the penetration level of the indenter after each measurement was different. This effect was much

more visible at the electron beam-treated substrate covered by TiN/TiO₂ due to the different surface roughness of the material. The indenter can touch a peak or a valley, and in the case of rough surfaces, the scattering of the level of penetration will be significant. The results show that the EBT of Co–Cr substrate led to a decrease in the hardness from 10.706 GPa (for untreated substrate) to 5.030 GPa (for treated substrate). According to the authors of [43,44], when (111) planes in polycrystalline TiN films are predominant, the hardness should be the highest. These statements are in agreement with the results of our study, where it was shown that electron beam treatment of Co–Cr substrate led to a reorientation of the microvolumes from (111) to denser (200) planes of TiN film, triggering a decrease in the microhardness values. It should be noted that, at depths of penetration of the indenter above 10%, the measured values are influenced by the hardness of the substrate. From the load–displacement curves, it is visible that the indenter penetration depth reached about 50%–60% of the coating thickness in both cases, which meant that the measured values were affected by the base material. On the other hand, it was found that treatment of Co–Cr alloy by high-energy fluxes caused a significant increase in the hardness [29], which is contrary to our results. Therefore, the influence of the orientation of microvolumes of layers on the discussed mechanical characteristic of TiN/TiO₂ coating should be significantly higher compared to the properties of the substrate.

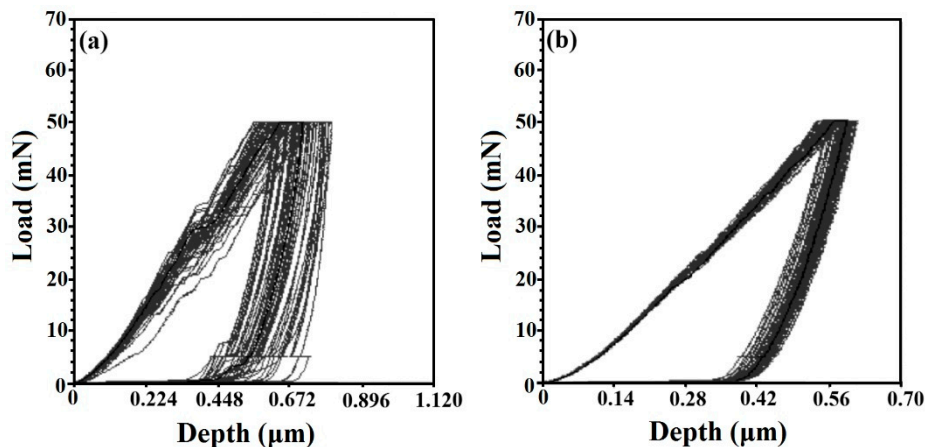


Figure 5. Penetration curves of the indenter of (a) TiN/TiO₂ coating deposited on treated Co–Cr substrate and (b) TiN/TiO₂ coating deposited on untreated Co–Cr substrate.

In the case of deposition of coatings for the manufacturing of implants, their mechanical properties should be similar to those of human bones. Otherwise, an effect related to severe stress shielding will appear. As mentioned above, the hardness of the bilayer TiN/TiO₂ deposited on untreated Co–Cr substrate was 10 GPa, and this value is quite high compared to those of human bones. Thus, it is clear that such coatings are not appropriate for implant manufacturing. After the EBT of Co–Cr substrate, the hardness of TiN/TiO₂ coating was reduced to 5 GPa, which is in agreement with the results published in [45] and is comparable with the measured values for human teeth [46].

The COF on the surfaces of both samples was measured by wear test at a load of 2 N and for 600 s, and the results are shown in Figure 6. Also, the mean friction coefficients of the investigated specimens are summarized in Table 2. The results obtained by wear investigations revealed that the COF was about 0.65 in the case of deposition of bilayer TiN/TiO₂ on untreated Co–Cr and significantly decreased down to 0.24 when the same coating was deposited on an EBT substrate. For a better understanding of the friction behavior of the deposited coatings, the experimentally obtained friction curves were extensively analyzed. At the starting point, the COF of both specimens was very similar, reaching values of 0.18. In the case of the bilayer TiN/TiO₂ deposited on the untreated substrate, COF increased gradually with increasing sliding time (to about 150 s) and reached values of about 0.8. Also, some fluctuations in the COF were visible in the later stages of the wear test up to 300 s, suggesting the formation of debris. With regard to the sample with deposited bilayer TiN/TiO₂ on

electron beam-treated substrate, the coefficient of friction was about 0.15 in the beginning and increased constantly during the measurement, up to about 0.4. No fluctuations were registered, meaning that the deposited coating on electron beam-treated Co–Cr was significantly more ductile compared to the untreated substrate. As already mentioned, TiN surface with (200) orientation exhibits much more affinity to oxidation and provides available sites for oxygen molecule adsorption. This means that the zone between the nitrogen and oxygen part of the coating (i.e., the oxynitride region) should be larger due to the diffusion of the oxygen in the TiN layer [34], meaning that the thickness of the oxide–nitride layer should be a bit larger in the case of deposition on the treated substrate. It follows that the coating deposited on EBT substrate can be characterized with higher ductility, which is in agreement with the results for the coefficient of friction.

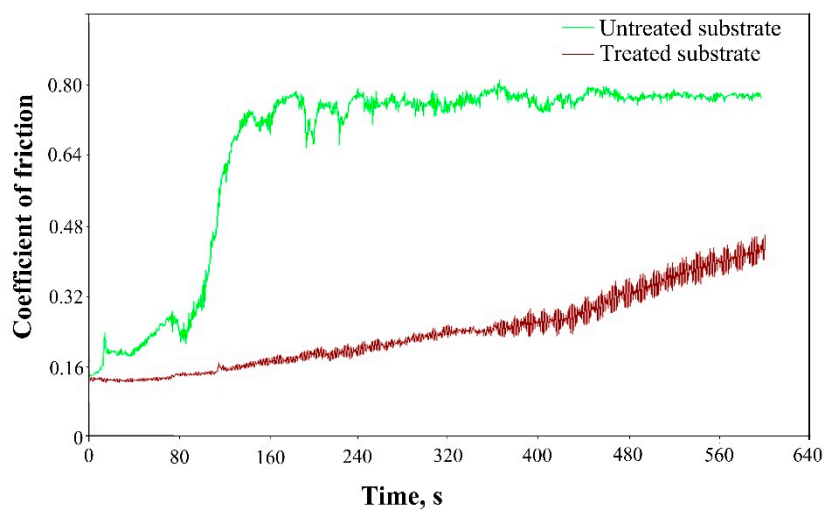


Figure 6. Coefficient of friction of bilayer TiN/TiO₂ coatings deposited on electron beam-treated and untreated Co–Cr substrate.

The results of the present study show the possibility of controlling the structure and properties of multilayer TiN/TiO₂ coatings deposited on Co–Cr substrates by means of electron beam treatment. It was found that the treatment process led to structural changes in the base Co–Cr material, which corresponded to an alteration in the film growth mechanism of the multilayer coating and corresponding mechanical properties. It is known that the electron beam surface treatment technology is an appropriate technique for surface modification, and it has several advantages compared to traditional manufacturing methods, such as annealing. The heating and cooling rates on the surface are quite high, and the changes in the structure and functional properties can be easily controlled, which is important for exploitation. The input energy during the treatment can be accurately dosed, which allows a strict control on structural modifications. Furthermore, materials with complex shape can be easily manufactured, while traditional techniques involve processing these parts separately and then assembling them. It should be noted that the application of electron beam-treated materials in practice has continuously increased, and more and more industrial companies have introduced this technique during the last decades.

4. Conclusions

The results obtained in the present study show the effect of electron beam treatment processing of Co–Cr substrates on the film growth, mechanical properties, and surface topography of multilayer TiN/TiO₂ coatings deposited by reactive magnetron sputtering. It was shown that electron beam treatment of the substrate led to a change in its phase composition from a double-phase structure of ϵ -Co and γ -Co to a single-phase structure of γ -Co. The deposited TiN/TiO₂ coatings were monophasic and polycrystalline, and the results showed the presence of anatase TiO₂ and TiN phases. It was found that electron beam treatment of the substrate led to a reorientation in the microvolumes from (111) to

(200) at the TiN phase. The EBT of the base material caused a change in the growth mechanism of the TiN phase from the three-dimensional Volmer–Weber to the layer-by-layer Frank–van der Merwe mechanism. Such reorientation of the microvolumes was not observed for TiO₂. It was found that electron beam treatment did not significantly affect the thickness of the coatings and the deposition rate. After EBT, the surface roughness increased from about 5–15 nm for the deposited coatings. The higher surface roughness after the EBT process led to an increase in the contact area, which might support cell growth and adhesion on the surface of the deposited bilayer coating. It was demonstrated that electron beam surface treatment tended to decrease the hardness of the deposited films from about 10–5 GPa. The observed decrease in the hardness was attributed to the change in the preferred crystallographic orientation and film growth mechanism. The hardness of the bilayer coating after the EBT of the Co–Cr substrate was much closer to that of human bones, which means that severe stress shielding effect could not be expected. The evaluated COF exhibited significantly lower values in the case of EBT of the substrate compared to the untreated Co–Cr material.

Author Contributions: Conceptualization, S.V., S.P. and P.P.; Formal Analysis, A.A., M.N. and R.B.; Investigation, S.V., A.A., R.B., M.N., D.D. and N.I.; Writing—Original Draft Preparation, S.V.; Writing—Review and Editing, M.N. and P.P.

Funding: This research was funded by the Bulgarian National Science Fund (project No. DN 17/17-2017).

Acknowledgments: The authors would like to express their sincere thanks to Slavcho Topalski from Fraunhofer-Institut für Werkstoff- und Strahltechnik IWS for his assistance in GDOES measurements.

Conflicts of Interest: The authors declare no conflict of interest.

References

1. Cobb, A.; Schmalzreid, T. The clinical significance of metal ion release from cobalt-chromium metal-on-metal hip joint arthroplasty. *Proc. Inst. Mech. Eng. H* **2006**, *220*, 385–398. [[CrossRef](#)] [[PubMed](#)]
2. Shetty, V.; Villar, R. Development and problems of metal-on-metal hip arthroplasty. *Proc. Inst. Mech. Eng. H* **2006**, *220*, 371–377. [[CrossRef](#)] [[PubMed](#)]
3. Martinez-Nogues, V.; Nesbitt, J.; Wood, R.; Cook, R. Nano-scale wear characterization of CoCrMo biomedical alloys. *Tribol. Int.* **2016**, *93*, 563–572. [[CrossRef](#)]
4. Wooley, P.; Schwarz, E. Aseptic loosening. *Gene Ther.* **2004**, *11*, 402–407. [[CrossRef](#)] [[PubMed](#)]
5. Fu, Y.; Hu, J.; Shen, X.; Wang, Y.; Zhao, W. Surface hardening of 30CrMnSiA steel using continuous electron beam. *Nucl. Instr. Meth. Phys. Res. B* **2017**, *410*, 207–214. [[CrossRef](#)]
6. Fu, J.; Hu, J.; Huo, W.; Cao, X.; Zhang, R.; Zhao, W. Characterization of high-current pulsed electron beam interaction with AISI 1045 steel and the microstructure evolution. *Procedia CIRP* **2018**, *68*, 196–199. [[CrossRef](#)]
7. Fu, Y.; Hu, J.; Zhang, X.; Huo, W.; Cao, X.; Zhao, W. Surface modification of AISI 1045 steel by pseudospark based pulsed electron beam. *Nucl. Instr. Meth. Phys. Res. B* **2018**, *434*, 88–92. [[CrossRef](#)]
8. Grishunin, V.; Gromov, V.; Ivanov, Y.; Teresov, A.; Konovalov, S. Evolution of the phase composition and defect substructure of rail steel subjected to high-intensity electron-beam treatment. *J. Surf. Investig. X-ray Synchrotron Neutron Tech.* **2013**, *7*, 990–995. [[CrossRef](#)]
9. Gromov, V.; Vorobiev, S.; Konovalov, S.; Romanov, D.; Ivanov, Y.; Semina, O.; Kazimirov, S. Increase in fatigue life of steels by electron-beam processing. *J. Surf. Investig. X-ray Synchrotron Neutron Tech.* **2016**, *10*, 83–87. [[CrossRef](#)]
10. Vilar, R.; Almeida, A. Laser surface treatment of biomedical alloys. In *Laser Surface Modification of Biomaterials: Techniques and Applications*, 1st ed.; Vilar, R., Ed.; Woodhead Publishing: Cambridge, UK, 2016; pp. 35–75.
11. Ramskogler, C.; Warchomicka, F.; Mostofi, S.; Weinberg, A.; Sommitsch, C. Innovative surface modification of Ti6Al4V alloy by electron beam technique for biomedical application. *Mater. Sci. Eng. C* **2017**, *78*, 105–113. [[CrossRef](#)]
12. Lei, L.; Shi, C.; Zhou, S.; Gu, Z.; Zhang, L. Enhanced corrosion and wear resistance properties of carbon fiber reinforced Ni-based composite coating by laser cladding. *Surf. Coat. Technol.* **2018**, *334*, 274–285. [[CrossRef](#)]
13. Shi, C.; Lei, J.; Zhou, S.; Dai, X.; Zhang, L. Microstructure and mechanical properties of carbon fibers strengthened Ni-based coatings by laser cladding: The effect of carbon fiber contents. *J. Alloy. Compd.* **2018**, *744*, 146–155. [[CrossRef](#)]

14. Han, J. Recent progress in thin film processing by magnetron sputtering with plasma diagnostics. *J. Phys. Appl. Phys.* **2009**, *42*, 043001. [[CrossRef](#)]
15. Kelly, P.; Arnell, R. Magnetron sputtering: A review of recent developments and applications. *Vacuum* **2000**, *56*, 159–172. [[CrossRef](#)]
16. Arnell, R.; Kelly, P. Recent advances in magnetron sputtering. *Surf. Coat. Technol.* **1999**, *112*, 170–176. [[CrossRef](#)]
17. Safi, I. Recent aspects concerning DC reactive magnetron sputtering of thin films: A review. *Surf. Coat. Technol.* **2000**, *127*, 203–218. [[CrossRef](#)]
18. Johnson, M.; Cote, P. Modeling magnetron sputter deposition. *Mater. Manuf. Proc.* **2006**, *21*, 628–633. [[CrossRef](#)]
19. Datta, S.; Das, M.; Krishna Balla, V.; Bodhak, S.; Murugesan, V. Mechanical, wear, corrosion and biological properties of arc deposited titanium nitride coatings. *Surf. Coat. Technol.* **2018**, *344*, 214–222. [[CrossRef](#)]
20. Pham, V.; Jun, S.; Kim, H.; Koh, Y. Deposition of titanium nitride (TiN) on Co–Cr and their potential application as vascular stent. *Appl. Surf. Sci.* **2012**, *258*, 2864–2868. [[CrossRef](#)]
21. Chen, L.; Xu, T.; Lu, S.; Wang, Z.; Chen, S.; Zhang, L. Improved hardness and wear resistance of plasma sprayed nanostructured NiCrBSi coating via short-time heat treatment. *Surf. Coat. Technol.* **2018**, *350*, 436–444. [[CrossRef](#)]
22. Chen, L.; Wang, H.; Zhao, C.; Lu, S.; Wang, Z.; Sha, J.; Chen, S.; Zhang, L. Automatic remelting and enhanced mechanical performance of a plasma sprayed NiCrBSi coating. *Surf. Coat. Technol.* **2019**, *369*, 31–43. [[CrossRef](#)]
23. Grumbt, G.; Zenker, R.; Biermann, H.; Weigel, K.; Bewilogua, K.; Breuer, G. Duplex surface treatment—physical vapor deposition (PVD) and subsequent electron beam hardening (EBH). *Adv. Eng. Mater.* **2014**, *16*, 511–516. [[CrossRef](#)]
24. Angelov, V.; Ormanova, M.; Kaisheva, D.; Lazarova, R.; Dimitrova, R.; Petrov, P. Selective electron beam surface alloying of aluminum with TiCN nanoparticles. *Nucl. Instr. Meth. Phys. Res. Sec. B* **2019**, *440*, 88–94. [[CrossRef](#)]
25. Ormanova, M.; Angelov, V.; Petrov, P. Investigation of the thermal processes in electron-beam surface modification by means of a scanning electron beam. *J. Phys. Conf. Ser.* **2016**, *700*, 012033. [[CrossRef](#)]
26. Granqvist, C.; Buhrman, R. Ultrafine metal particles. *J. Appl. Phys.* **1976**, *47*, 2200–2219. [[CrossRef](#)]
27. Mani, A.; Salinas-Rodriguez, A.; Lopez, H. Deformation induced FCC to HCP transformation in a Co–27Cr–5Mo–0.05C alloy. *Mater. Sci. Eng. A* **2011**, *528*, 3037–3043. [[CrossRef](#)]
28. Wei, D.; Koizumi, Y.; Takashima, T.; Nagasako, M.; Chiba, A. Fatigue improvement of electron beam melting fabricated biomedical Co–Cr–Mo alloy by accessible heat treatment. *Mater. Res. Lett.* **2018**, *6*, 93–99. [[CrossRef](#)]
29. Wei, X.; Li, W.; Liang, B.; Li, B.; Zhang, J.; Zhang, L.; Wang, Z. Surface modification of Co–Cr–Mo implant alloy by laser interference lithography. *Tribol. Int.* **2016**, *97*, 212–217. [[CrossRef](#)]
30. Combadiere, L.; Machet, J. Reactive magnetron sputtering deposition of TiN films. I. Influence of the substrate temperature on structure, composition and morphology of the films. *Surf. Coat. Technol.* **1996**, *88*, 17–27. [[CrossRef](#)]
31. Shapovalov, V.; Komlev, A.; Bondarenko, A.; Baykov, P.; Karzin, V. Substrate heating and cooling during magnetron sputtering of copper target. *Phys. Lett. A* **2016**, *380*, 882–885. [[CrossRef](#)]
32. Glagoleva, Y.; Polev, V.; Gorbатов, V.; Ivliev, A.; Kurichenko, A.; Taluts, S.; Korshunov, I. Thermal and kinetic properties of cobalt–chromium alloys at high temperatures. *Phys. Met. Metall.* **2009**, *107*, 254–261. [[CrossRef](#)]
33. Iordanova, I.; Kelly, P.; Mirchev, R.; Antonov, V. Crystallography of magnetron sputtered TiN coatings on steel substrates. *Vacuum* **2007**, *81*, 830–842. [[CrossRef](#)]
34. Seifitokaldani, A.; Savadogo, O.; Perrier, M. Density functional theory (DFT) computation of the oxygen reduction reaction (ORR) on titanium nitride (TiN) surface. *Electroch. Acta* **2014**, *141*, 25–32. [[CrossRef](#)]
35. Hu, J.; Zhang, G.; Xu, H.; Chen, Y. Microstructure characteristics and properties of 40Cr steel treated by high current pulsed electron beam. *Mater. Technol.* **2012**, *27*, 300–303. [[CrossRef](#)]
36. Zhang, K.; Zou, J.; Grosdidier, T.; Gey, N.; Weber, S.; Yang, D.; Dong, C. Mechanisms of structural evolutions associated with the high current pulsed electron beam treatment of a NiTi shape memory alloy. *J. Vac. Sci. Technol. A* **2007**, *25*, 28–36. [[CrossRef](#)]

37. Mendonça, G.; Mendonça, D.; Aragao, F.; Cooper, L. Advancing dental implant surface technology—From micron- to Nanotopography—Review. *Biomaterials* **2008**, *29*, 3822–3835. [[CrossRef](#)]
38. Zhou, W.; Zhong, X.; Wu, X.; Yuan, L.; Zhao, Z.; Wang, H.; Xia, Y.; Feng, Y.; He, J.; Chen, W. The effect of surface roughness and wettability of nanostructured TiO₂ film on TCA-8113 epithelial-like cells. *Surf. Coat. Technol.* **2006**, *200*, 6155–6160. [[CrossRef](#)]
39. Silva, T.; Machado, D.; Viezzer, C.; Júnior, A.; Oliveira, M. Effect of titanium surface roughness on human bone marrow cell proliferation and differentiation: An experimental study. *Acta Cir. Bras.* **2009**, *24*, 200–205. [[CrossRef](#)]
40. Colon, G.; Ward, B.; Webster, T. Increased osteoblast and decreased Staphylococcus epidermidis functions on nanophase ZnO and TiO₂. *J. Biomed. Mater. Res. A* **2006**, *78*, 595–604. [[CrossRef](#)]
41. Oliver, W.; Pharr, G. An improved technique for determining hardness and elastic modulus using load and displacement sensing indentation experiments. *J. Mater. Res.* **1992**, *7*, 564–1583. [[CrossRef](#)]
42. Oliver, W.; Pharr, G. Measurement of hardness and elastic modulus by instrumented indentation: Advances in understanding and refinements to methodology. *J. Mater. Res.* **2004**, *19*, 3–20. [[CrossRef](#)]
43. Reed-Hill, R.; Abbachian, R. *Physical Metallurgy Principles*, 3rd ed.; PWS Publishing Company: Boston, MA, USA, 1994.
44. Ackerland, D. *The Science and Engineering of Materials*; PWS Engineering: Boston, MA, USA, 1985.
45. Bait, L.; Azzouz, L.; Madaoui, N.; Saoula, N. Influence of substrate bias voltage on the properties of TiO₂ deposited by radio-frequency magnetron sputtering on 304L for biomaterials applications. *Appl. Surf. Sci.* **2017**, *395*, 72–77. [[CrossRef](#)]
46. Gutiérrez-Salazar, M.; Reyes-Gasga, J. Microhardness and chemical composition of human tooth. *Mater. Res.* **2003**, *6*, 367–373. [[CrossRef](#)]



© 2019 by the authors. Licensee MDPI, Basel, Switzerland. This article is an open access article distributed under the terms and conditions of the Creative Commons Attribution (CC BY) license (<http://creativecommons.org/licenses/by/4.0/>).